THE ASTROPHYSICAL JOURNAL, 350:266–274, 1990 February 10

COMPARATIVE MORPHOLOGICAL ANALYSIS OF PUPPIS A AT RADIO, INFRARED, OPTICAL, AND X-RAY WAVELENGTHS

RICHARD G. ARENDT[1] AND ELI DWEK
Laboratory for Astronomy and Solar Physics, NASA/Goddard Space Flight Center
ROBERT PETRE
Laboratory for High Energy Astrophysics, NASA/Goddard Space Flight Center
JOHN R. DICKEL
Department of Astronomy, University of Illinois
ROBERT S. ROGER
Dominion Radio Astrophysical Observatory
AND
DOUGLAS K. MILNE AND MICHAEL J. KESTEVEN
Division of Radiophysics, CSIRO
Received 1989 May 16; accepted 1989 August 15

ABSTRACT

We present a new radio image of the supernova remnant Puppis A obtained with the Molonglo Observatory synthesis telescope (MOST) and the Parkes telescope, and infrared images of Puppis A and its surrounding medium obtained with the *IRAS*. We compare the remnant morphologies at radio, infrared, optical, and X-ray wavelengths. The radio image, which includes large-scale emission, shows a clumpy shell of emission with moderate central brightness. The infrared observations have the advantage of offering a detailed look at the medium into which the remnant is expanding. From the IR data, we find evidence of the remnant's expansion into a strong density gradient (distinct from the more gentle gradient of the Galactic plane), which had been inferred from previous X-ray observations. A strong, previously believed, isolated knot of enhanced X-ray and radio emission is a region of enhanced infrared emission as well, and it is part of a larger molecular complex with which the remnant is interacting.

Detailed correlative analysis of the infrared, radio, and X-ray emission shows that the IR emission correlates very well with the X-ray emission, confirming the idea that the IR emission arises from dust that is collisionally heated by the shocked gas.

Subject headings: infrared: sources — nebulae: individual (Puppis A) — nebulae: supernova remnants — radio sources: general — X-rays: sources

I. INTRODUCTION

In this study, we aim to discover the structure of the interstellar medium (ISM) in the vicinity of the supernova remnant (SNR) Puppis A (G260.4−3.4) and to determine how that structure influences the appearance of Puppis A in various spectral regimes. The infrared (IR) observations by the *Infrared Astronomical Satellite* (*IRAS*) are of particular interest in this work. The survey of the infrared sky by the *IRAS* (Neugebauer *et al.* 1984) provides a wealth of new information on the structure of the Galactic interstellar medium and on the dust which pervades it. The review by Beichman (1987) describes the wide variety of Galactic sources seen by the *IRAS*. Thermal radiation from interstellar dust appears in the IR regardless of the heating mechanism (radiative or collisional) or the state of the gas in which the dust is immersed (molecular, atomic, or ionized). Thus, in the IR we can examine a number of rather different environments (such as SNRs and interstellar clouds) simultaneously. While some information can be gleaned from the IR data alone, the greatest results are found through comparison of the IR data with radio, optical, and X-ray data. With such a multiwavelength analysis, we can separate and identify different sources of emission and determine how these sources relate to the SNR. The changes in appearance across the spectrum will also provide information on the physical processes responsible for the IR emission of Puppis A.

The *IRAS* data always reveal the ISM in the direction of any SNR, but in only a few cases are we afforded a clear view of the SNR itself. Many SNRs are entirely hidden by emission from other sources along the line of sight (see Arendt 1989). However, Puppis A is well suited for this study, because it is a relatively strong and unconfused IR source. These favorable conditions are due to the high Galactic latitude ($b = -3.^{\circ}4$) of Puppis A, which places it away from much of the confusion of the Galactic plane. Its angular size ($\sim 56'$ diameter) is small enough so that the number of overlapping sources is small, but the SNR is still large enough that interesting detail can be resolved by the *IRAS*. Puppis A is also one of the brightest SNRs in the radio and X-ray regimes (see listings by Green 1988 and Seward 1988). Therefore, it has been studied frequently in regions of the spectrum outside the IR. This provides a context for the interpretation of the IR data. Previous work has established an age of ≤ 5000 yr for Puppis A (e.g., Milne, Goss, and Danziger 1983; Winkler *et al.* 1988). This is young enough that clumps of ejecta from the original blast can still be identified (Winkler and Kirshner 1985), but old enough that interactions with the ISM have had time to create the very asymmetrical appearance of the SNR at all wavelengths. This asymmetry is presumed to arise from a density gradient in the

[1] National Research Council/Resident Research Associate.

ISM (Petre *et al.* 1982). The local ISM near Puppis A has a mean density of ~ 1 cm^{-3} with several notable large and small scale variations (Petre *et al.* 1982). Indications of these variations are apparent in the IR data. A distance of ~ 2 kpc, suggested by $\Sigma - D$ relations (Milne 1979; Caswell and Lerche 1979), is commonly accepted for Puppis A. An analysis of X-ray data by Szymkowiak (1985) yields a distance of ~ 2.5 kpc, although an earlier study of the X-ray emission (Zarnecki *et al.* 1978) suggests a distance of only ~ 1 kpc.

In the next section, we describe briefly the data and relevant steps in the data reduction. More details on the data and processing can be found in the referenced works. In § III, we discuss the morphology of Puppis A and its surrounding medium at radio, IR, optical, and X-ray wavelengths. Significant similarities and differences across this wide sampling of the spectrum are noted. In § IV, we state the conclusions about the structure of the SNR and its local ISM that can be found through these comparisons. Since they are qualitative in nature, our conclusions are independent of the details of the background subtraction applied to the IR data. Infrared background levels for extended sources in the galactic plane are often difficult to judge and can have strong consequences for quantitative results. In a subsequent paper, we will use the IR data to derive detailed results which are found to depend on the assumed background emission.

II. DATA REDUCTION

a) Radio Data

Observations of the radio emission at 843 MHz from Puppis A were made with the Molonglo Observatory synthesis telescope (MOST) of the University of Sydney in 1983 February and with the Parkes 64 m radio telescope in 1983 October. The MOST is a synthesis interferometer comprising two colinear cylindrical paraboloids aligned east-west, each 800 m in extent (Mills 1981). A map is produced in real time by the overlaying of the outputs of a comb of fan beams, which tracks the field center over a period of 12 hr. The synthesized half-power beamwidth is 44″ (right ascension) by 44″ cosec δ (declination) within a field of 70′ by 70′ cosec δ. The synthesized beam produced by this method has one major sidelobe of $\sim 8\%$ intensity, the effects of which are removed by a special adaptation of the CLEAN technique (Roger *et al.* 1984). An image of Puppis A made from the MOST data alone appears in the work by Kesteven and Caswell (1987).

Because of a gap between the east and west paraboloids of the MOST, maps of extended emission are deficient in structure of a scale $>20'$. To obtain this structure, Puppis A was observed with the Parkes telescope, which has a half-power beamwidth of 23′ at 843 MHz. The Parkes observations were calibrated using PKS 0915−11 (Hydra A), with an assumed flux density of 70 Jy at 843 MHz. The total flux density of Puppis A, determined from these observations but corrected for point sources in the field, is 148 ± 10 Jy. This value was used as a constraint in the combining process to create the composite map, in the manner described by Roger *et al.* (1984). The composite map from both sets of observations is shown in Figure 1*a*.

For comparison with the lower resolution IR data, a smoothed version of the radio image was produced. The smoothed radio image (Fig. 1*b*) has approximately the same resolution as the 60 μm IR data, although the beam shape is slightly different.

b) Infrared Data

The infrared observations were part of the complete sky survey carried out by the *IRAS* (Neugebauer *et al.* 1984). The data used here were processed with the standard "coadding" techniques used at the Infrared Processing and Analysis Center (IPAC). There is one image corresponding to each of the four broad-wavelength bands observed by the *IRAS* (12, 25, 60, and 100 μm). The coadded fields used here are $2^\circ \times 2^\circ$. The pixel sizes are 15″, 15″, 30″, and 60″ for the images in the 12, 25, 60, and 100 μm bands, respectively. Each coadded image is an average of the data from each of the satellite's scans over the region of Puppis A. Near Puppis A, all of the scans are nearly parallel; thus, the effective beam in each of the bands has a reasonable shape which can be characterized as Gaussian. An indication of the beam size is provided by the bright point-like source *IRAS* 08247−4223 (at $\alpha = 8^{\rm m}24^{\rm m}43^{\rm s}.1$, $\delta = -42^\circ 23' 10''$) which appears in all four bands. Gaussian fits to this source indicate the resolutions quoted in Table 1. The coadded images are in units of W m^{-2} sr^{-1}. As part of the "coaddition" process, a bias level is removed from each of the images so that the estimated zero level corresponds to the lower quartile of pixel intensity values. We made a further adjustment by subtracting a tilted planar background from each of the four images. In all cases, the gradient of the background was in the direction toward the Galactic plane. The estimated errors in the IR data after background removal are: 7.5, 3.5, 5.5, and 5.5×10^{-8} W m^{-2} sr^{-1} for the 12, 25, 60, and 100 μm bands, respectively. These values are near the level of the first or second positive contours of the maps shown in Figure 2.

c) Optical Data

The optical image shown in Figure 3 is a portion of the Hα and [N II] plate presented by Elliott, Goudis, and Meaburn (1976). Comparison of the optical and radio emission is found in the work of Goudis and Meaburn (1978). Here it has been reproduced on approximately the same scale as the other maps of Puppis A. Contours and coordinates from the 60 μm infrared image are superimposed on the image. The crosses mark the positions of SAO stars, which were used for alignment.

d) X-Ray Data

The X-ray data were collected by the High Resolution Imager (HRI) aboard the Einstein Observatory (Giacconi *et al.* 1979). The HRI is sensitive to X-rays in the energy range from ~ 0.1 to 4.0 keV. Due to the limited field of view of the HRI, Petre *et al.* (1982) created a mosaic of several images which covers the entire SNR except for a small portion on the southwest edge. A thorough analysis and excellent illustrations of these data are found in the paper by Petre *et al.* (1982). Here we use the same mosaic, but to make a fair comparison we have convolved the image with a Gaussian function so that its resolution matches that of the 60 μm IR data. A lack of isolated

TABLE 1

IRAS RESOLUTION ESTIMATED FROM IRAS 08247−4223

Wavelength (μm)	Full Width at Half-Maximum	Position Angle
12	4.′71 × 1.′76	118°
25	4.74 × 1.63	118
60	5.35 × 2.29	115
100	5.60 × 4.37	118

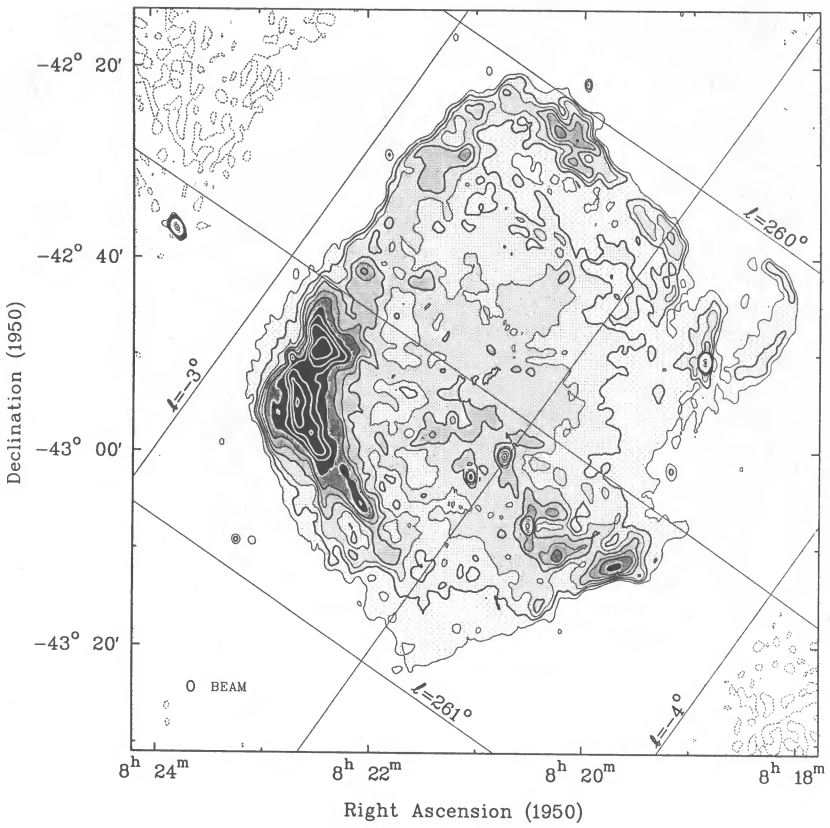

FIG. 1*a*

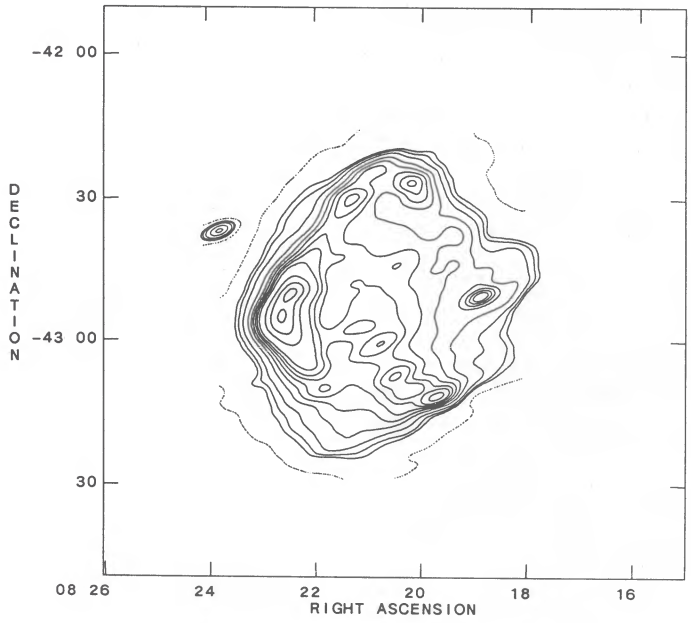

FIG. 1*b*

FIG. 1.—(*a*) Puppis A at 843 MHz. The full-resolution data are illustrated here. A clumpy shell structure is seen along with significant emission across the face of the shell. Contour levels are at −20 (*dashed*), 20, 35, 50, 70, 95, 125 (*black*), 170, 230, 300, 400, and 530 (*white*) mJy beam^{-1}. (*b*) Puppis A at 843 MHz after the image has been smoothed to match the resolution of the 60 μm IR data (5′.35 × 2′.29). Contour levels are at −87.8, 43.8, 87.8, 176., 351., 527., 702., 878., 1050, 1320, 2190, 3080, and 3950 mJy per convolved beam.

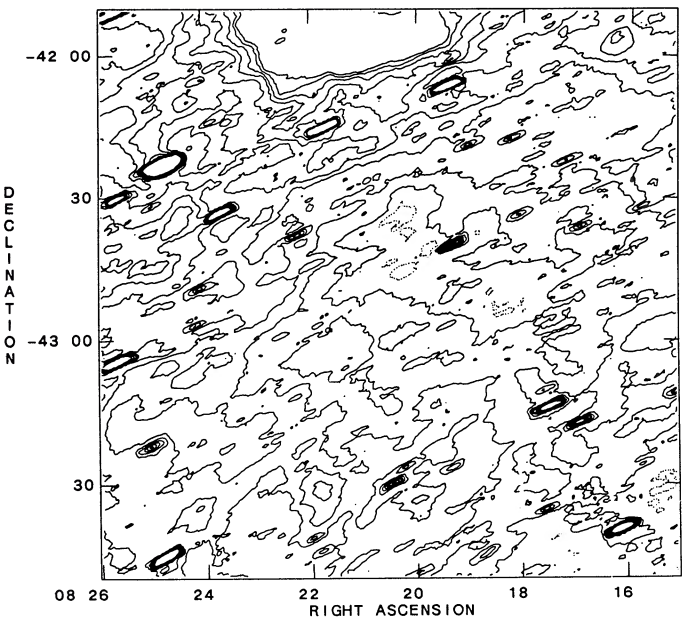

FIG. 2a

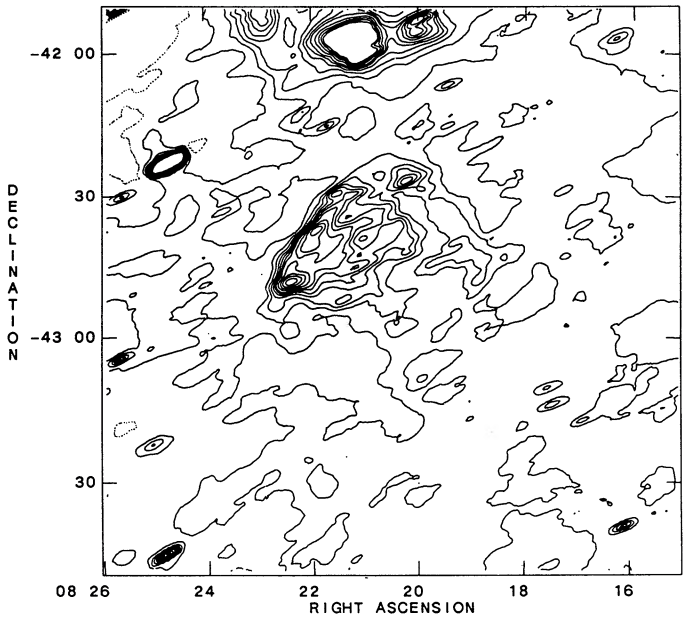

FIG. 2b

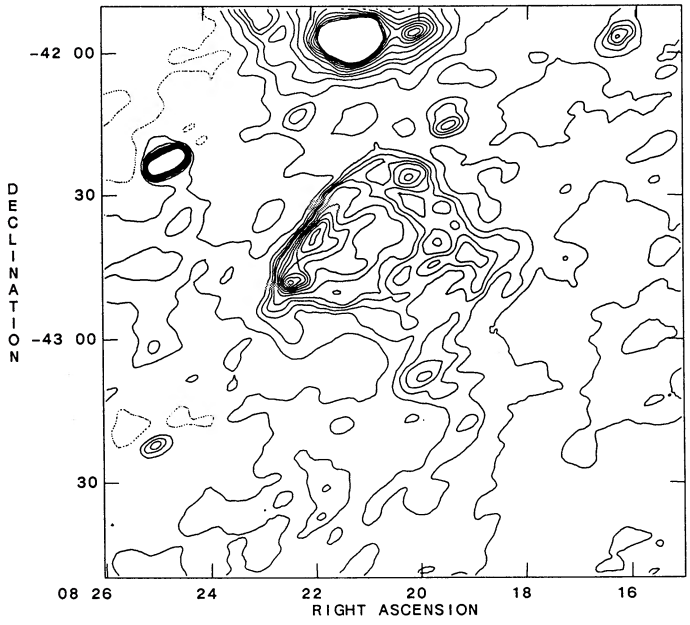

FIG. 2c

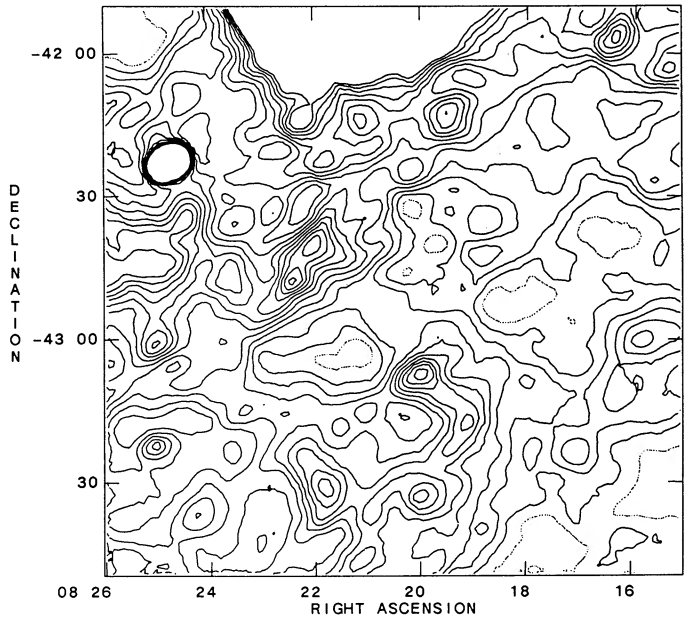

FIG. 2d

FIG. 2.—Background subtracted images of Puppis A in the four *IRAS* bands. (*a*) 12 μm contour levels are at -5, 0, 5, 10, 15, 20, 25, 30, 35, and 40×10^{-8} W m^{-2} sr^{-1}. (*b*) 25 μm contour levels are at -3.5, 0, 3.5, 7, 10.5, 14, 17.5, 21, 28, 35, 42, and 49×10^{-8} W m^{-2} sr^{-1}. (*c*) 60 μm contour levels are at -5.5, 0, 5.5, 11, 16.5, 22, 27.5, 33, 44, 55, 66, 77, 88, and 99×10^{-8} W m^{-2} sr^{-1}. (*d*) 100 μm contour levels are at -2.75, 0, 2.75, 5.5, 8.25, 11, 13.75, 16.5, 19.25, 22, 24.75, and 27.5×10^{-8} W m^{-2} sr^{-1}.

point sources in the X-ray field prevents us from checking the resolution of the smoothed image as was done with the infrared data. However, the very similar appearance of several features of the SNR in both the smoothed X-ray and the IR data indicates that the resolution of the images is comparable. The smoothed X-ray image is shown in Figure 4.

III. MORPHOLOGY AT VARIOUS WAVELENGTHS

The radio emission of Puppis A displays a fairly complete, clumpy shell structure. Only a few locations around the edge of the SNR, at the south and southwest, show no limb brightening. The central portion exhibits relatively bright, large-scale emission, equalling the brightness of some portions of the shell. The strongest radio emission is found in the region of the "eastern knot" and the "hook." (All the features discussed in this paper are identified in Fig. 5, which is a map of selected contours of the 60 μm emission of Puppis A.) The peak brightness of these features is $\sim$3 times that of any other portion of the shell. The outer edges of the SNR are unusually straight, particularly along the northeast and the northwest. There are

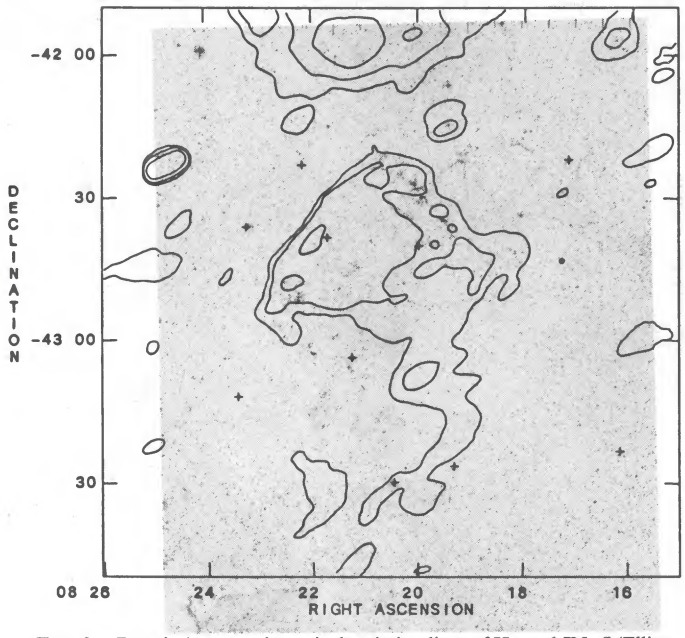

FIG. 3.—Puppis A as seen in optical emission lines of Hα and [N II] (Elliott, Goudis, and Meaburn 1976; Goudis and Meaburn 1978). Contours and coordinates are from the 60 μm IR data. Brightest knots and filaments lie along the northwest edge of the SNR. Other emission is scattered across the SNR. Crosses mark the positions of SAO stars used for alignment.

only a few indications of the long filaments which are often found in SNRs such as the Cygnus Loop, IC 443 and CTB1 (Straka *et al.* 1986; Mufson *et al.* 1986; Dickel and Willis 1980). The five bright point sources in the image are believed to be unrelated to Puppis A (Milne, Goss, and Danziger 1983).

The infrared morphology of Puppis A is clearest at 60 μm. The SNR appears almost identical at 25 μm, except for being

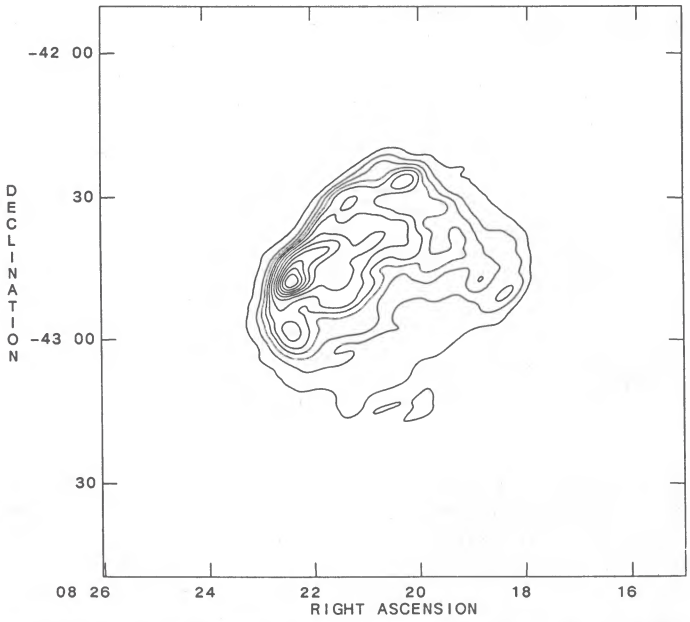

FIG. 4.—Puppis A as seen in the soft X-ray emission (~0.1 to 4 keV) observed by the Einstein Observatory's High Resolution Imager. This image has been smoothed to match the resolution of the 60 μm IR data. Contour levels are at 0.008, 0.016, 0.025, 0.035, 0.045, 0.06, 0.08, 0.10, 0.12, 0.14, 0.16, and 0.18 counts s^{-1} $arcmin^{-2}$.

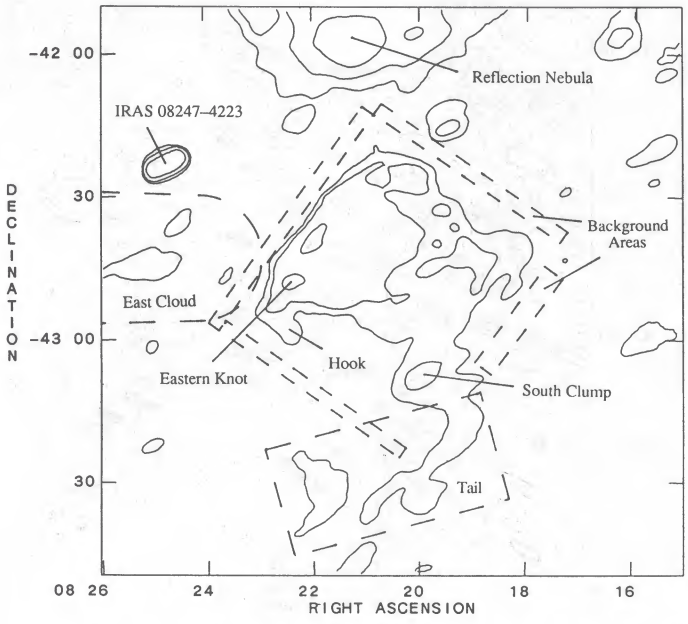

FIG. 5.—Contour map of Puppis A and its surroundings at 60 μm. The locations of features discussed in the text are indicated. The four narrow boxes indicate the regions that were chosen as representative of the local background level.

relatively fainter compared to the surroundings. The only 12 μm emission from Puppis A appears as a weak peak at the location of the eastern knot. At 100 μm, the SNR is more confused by background clouds than at 25 or 60 μm. Overall, the appearance of Puppis A seems to be the same in all four IR bands, but the SNR is more heavily confused at long and at short wavelengths.

Other features of interest in the IR images are the confusing sources themselves. We would like to know if any of these sources are actually related to the SNR, or if they are only by chance along the same line of sight while differing greatly in distance. The IR data reveal the "east cloud" ($\alpha \geq 8^h23^m$, $-43°00' \leq \delta \leq -42°30'$) which abuts the SNR directly at the location of the bright eastern knot. This cloud corresponds to that seen at velocities near +16 km s^{-1} in the H I and CO data by Dubner and Arnal (1988). The "tail" to the south of Puppis A ($8^h19^m \leq \alpha \leq 8^h23^m$, $-43°45' \leq \delta \leq 43°10'$) is also visible in the IR images. This feature and the east cloud both appear in all four *IRAS* bands, and thus have rather different spectra from the SNR itself. These features are most clearly seen in the 100 μm contour map of Figure 2*d*. The tail also resembles the east cloud in that it has infrared emission and is associated with a bright section of the edge of the remnant (in this case, the "south clump"). However, the tail seems to extend across the south clump and toward the center of the remnant at low emission levels. This is most noticeable in the 12 and 100 μm images (see Figs. 2*a* and 2*d*), where the SNR is relatively faint. The diffuse radio emission of the SNR appears to be slightly brighter just to the east of this extension of the tail than elsewhere across the central regions of the Puppis A. There may be evidence of the tail at velocities of +10 and +12 km s^{-1} in the H I maps presented by Dubner and Arnal (1988). The bright, extended IR source to the north of Puppis A, is most likely a reflection nebula because of its strong blue emission and weaker red emission surrounding a group of blue stars on the ESO sky survey plates. The bright point source to

the northeast of Puppis A is listed in the *IRAS* Point Source Catalog (1985) as IRAS 08247−4223, and at 12 μm and 25 μm it is listed in the *IRAS* Small Scale Structures Catalog (1986) as IRAS X0825−423, but no associated source was found among the various optical and IR catalogs that were searched as part of the compilation of the *IRAS* catalogs. Finally, on the lower resolution Skyflux plates (as described in the *IRAS* Explanatory Supplement, 1985), which have not had any background emission removed, it is seen that Puppis A sits near the crest of a ridge of emission which runs roughly parallel to the Galactic equator at $b \cong -3°$ with a width (FWHM) of about 2° (see Fig. 6). The "ridge" is seen most clearly between the reflection nebula and the east cloud, but it may extend through these brighter sources as well.

Most of the features which are seen in the radio are also detected in the IR, but with very different relative intensities. The most striking differences are between the eastern knot, which is the brightest region in both the radio and IR, and the hook, which is equally bright in the radio but very faint in the IR. The diffuse radio emission at the southern end of the SNR has no corresponding IR emission. In contrast, the IR emission is more prominent than the radio emission across the central and northeastern regions of the SNR. In general, there is some correspondence between select bright radio and IR features of the remnant. However, there is no overall correlation between the IR and radio intensities across the remnant. This lack of IR-radio correlation is illustrated in Figure 7, which shows the IR versus the radio brightness plotted for each 30″ × 30″ pixel covering the SNR. Some small portions of the remnant do fall within localized regions in Figure 7: the hook corresponds to the group of points which define the lower edge of the distribution at $I(\text{radio}) > 1.55$ Jy beam^{-1}, while the eastern knot fills the region of $I(\text{radio}) > 1.55$ Jy beam^{-1} and $I(\text{IR}) > 0.2 \times 10^{-6}$ W m^{-2} sr^{-1}.

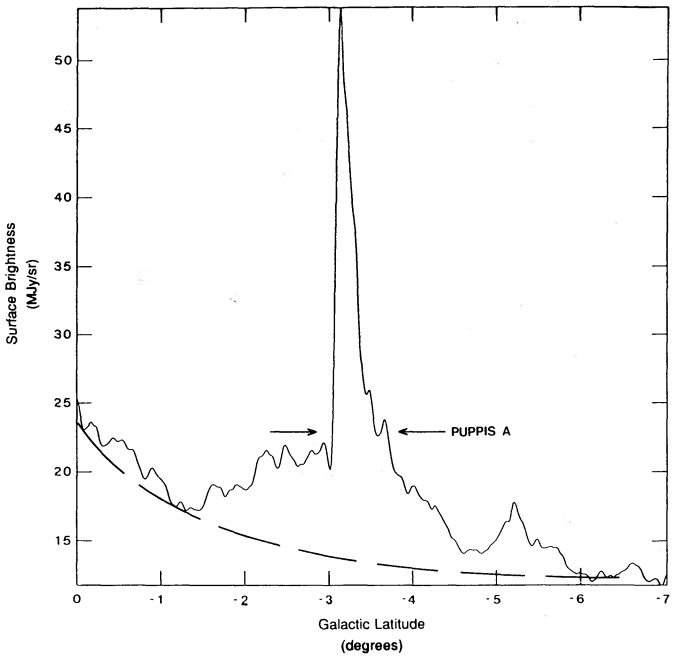

FIG. 6.—A slice showing the 60 μm surface brightness as a function of Galactic latitude at $l = 260.^{\circ}37$. Puppis A ($-3° > b > -4°$) sits near the peak of a ridge of emission ($-1.^{\circ}5 > b > -4.^{\circ}5$) that is separate from the general emission of the galactic plane (roughly indicated by the dashed line).

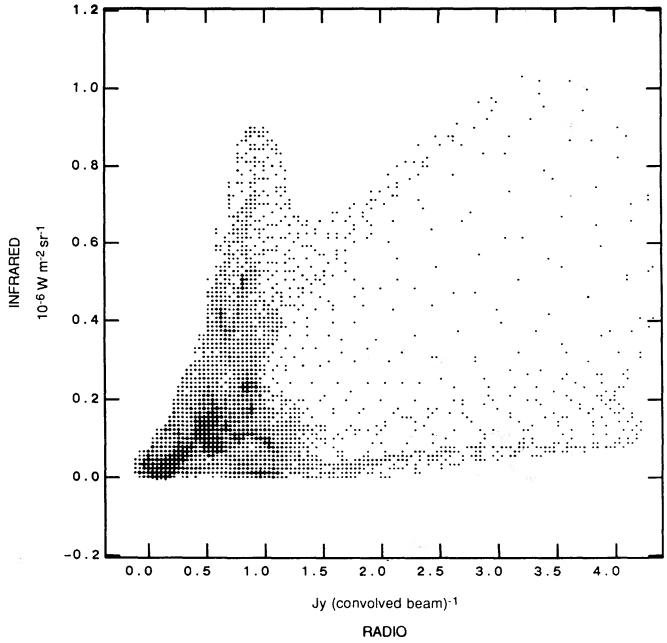

FIG. 7.—Correlation of the radio and IR emission. No consistent correlation appears between the smoothed 843 MHz radio intensity and the 60 μm IR intensity. Pixels (30″ × 30″) with radio brightnesses greater than 1.55 Jy per convolved beam are mostly from the eastern knot (bright IR emission) or from the hook (little or no IR emission). The scales on the axes can be related to the contour maps in Figs. 1*b* and 2*c*. The size of a plotted plus sign (" + ") in this figure scales as the number of pixels at that location.

The optical emission from Puppis A (Fig. 3) appears as clumps of knots and short filaments. Several of the brightest clumps lie along the northwest edge of the shell. One filament appears at the location of the eastern knot (see Petre *et al.* 1982; Petre and Teske 1987). Much of the optical emission is scattered across the SNR without clear relations to features seen at other wavelengths. Lack of correlation between radio and optical emission was noted by Milne, Goss, and Danziger (1983). Examination of the images presented here reveals that the IR and optical are not strongly correlated. Some filaments which lie to the northwest and outside the radio and IR boundaries of Puppis A, and others near the southern boundary of the remnant, show no radio or IR emission. A region of optical absorption is visible roughly at the location of the south clump (Goudis and Meaburn 1978).

The X-ray morphology of Puppis A exhibits a general intensity gradient across the remnant with an increase along the direction toward the northeast. There are two bright knots (the eastern knot and a feature at $\alpha \approx 8^{h}20^{m}14^{s}$, $\delta \approx -42°27'$) which were studied by Petre *et al.* (1982), and there is some filamentary structure. However, when smoothed to the resolution of the IR data, only the gradient, the bright knots, and some general clumpiness remain. The correlation of the X-ray and the radio emission is poor (Petre *et al.* 1982; Milne, Goss, and Danziger 1983). The correlation between the X-ray and IR emission is very good, however. Figure 8 illustrates this correlation by showing the plot of IR versus X-ray brightness for 30″ × 30″ pixels across the SNR. One exception from the general trend is the hook, where IR emission is weak despite moderate X-ray emission. Other regions show relative excesses of IR emission. The south clump shows IR emission but virtually no X-ray emission, and a small region along the north-

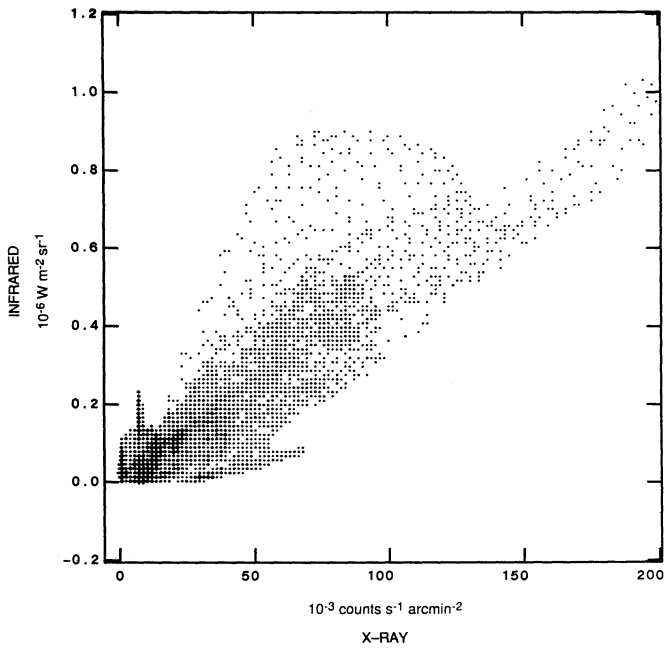

FIG. 8.—Correlation of X-ray and IR emission from Puppis A. Plotting the smoothed HRI X-ray vs. the 60 μm IR emission for 30″ × 30″ pixels clearly shows the good detailed correlation of the IR and X-ray emission. Scattered points lying above the general correlation are from a small IR-bright region on the northeast edge of the SNR. The scales on the axes can be related to the contour maps in Figs. 4 and 2*c*.

east rim of the SNR is very bright in the IR but of only moderate X-ray brightness. Petre *et al.* (1982) noted that there is very little detailed correlation between the X-ray and optical emission.

The good correlation of the IR and X-ray emission (Fig. 8), and poor correlations between the IR and radio (Fig. 7) and IR and optical emission, indicate that the bulk of the IR emission is from collisionally heated dust which resides in the hot plasma, and not from synchrotron radiation which would correlate with the radio synchrotron emission, atomic or ionic line emission, or thermal free-free emission from the denser optical knots and filaments. Errors in the IR background level would only affect the zero-intercept, not the slope, of the correlation between the X-ray and IR emission. The slope of the correlation, $\sim(4.9 \times 10^{-6}$ W m^{-2} sr$^{-2})/(1$ count s^{-1} arcmin$^{-2})$, corresponds to a ratio of (60 μm) IR to X-ray fluxes of ~ 1.7 (using conversion factors derived from Petre *et al.* 1982 and Dwek *et al.* 1987). Variations of this ratio by a factor of 2 or more can be found in particular regions of the SNR. Including the IR flux from the other bands will roughly double the ratio of IR to X-ray flux, which gives a result in agreement with the results of Dwek *et al.* (1987). The rough agreement between the observed flux ratio and the theoretically calculated value suggests that the dust is not significantly depleted in the shocked gas.

IV. DISCUSSION

The gradient in the intensity of the X-ray emission was attributed to a gradient in the ambient density in the region of Puppis A (Petre *et al.* 1982). This density gradient is steeper than that expected from the Galactic disk at this latitude, and it is probably caused by a ridge revealed by the IR emission (see Fig. 6). The H I data of Dubner and Arnal (1988) and the IR data indicate that this ridge probably corresponds to a larger region of more diffuse gas surrounding the east cloud. To the northwest, the ridge becomes confused by the bright reflection nebula. An association of these features is suggested by the H I data of Dubner and Arnal (1988). Dubner and Arnal find a local minimum in the H I emission (at velocities greater than 3 km s^{-1}) near the position of the reflection nebula. The stars illuminating the reflection nebula may be responsible for the H I hole either by ionizing the gas or by sweeping out the region with strong winds. The ridge widens to the southeast, where it includes the east cloud. Beyond there, it becomes confused with other diffuse IR emission.

The east cloud is responsible for causing the eastern X-ray/optical/IR/radio knot. This eastern knot marks the interface between the east cloud and the SNR. This knot was thought to be a swept-up dense cloud by Petre *et al.* (1982), who found a resemblance between the eastern knot and the cold cloud cores of the McKee and Ostriker (1977) model of the ISM. The *IRAS* data indicate, however, that the eastern knot is part of the larger east cloud, only marking the tip of this cloud. The east cloud is also seen in the recent H I and CO observations of Dubner and Arnal (1988). They point out that the velocity of the cloud (+16 km s^{-1}) places it at the same kinematic distance ($\sim$2.2 kpc) as Puppis A, confirming the association between cloud and remnant. At a distance of 2.2 kpc, the $\sim 30' \times 60'$ angular size of the east cloud indicates a radius of $\sim$14 pc. This would be one of the largest clouds to be found in the McKee and Ostriker model. The ridge is then larger than expected clouds, and its inferred density gradient is contrary to the notion of discrete components of the ISM with fixed temperatures and densities. We see no clear evidence of interaction with a low-density, high-temperature component of the ISM, which is presumed to have a large filling factor in the McKee and Ostriker model.

It appears that the tail is a cloud, or string of clouds, interacting with the SNR (perhaps at the south clump), but having a lower density than the east cloud. The lower density could account for the marginal (at best) detection of the tail in the H I data. The tail appears to wrap around from the south edge northward across either the front or back of the SNR. This accounts for weak radio and IR emission across the face of the SNR, with stronger emission near the south clump, where the interaction of the cloud and SNR presents a higher column density in the edge-on geometry. The most significant problem with this picture is the lack of enhanced X-ray emission at the south clump, in contrast to the strong X-ray emission at the eastern knot. The absorption region seen in the optical image suggests that at the location of the south clump, part of the IR emission is from a local cloud, closer to us than the east cloud and the rest of the tail, neither of which show such obvious absorption. It may be that some of the X-rays are absorbed by this local cloud. This cloud is not visible in the H I and CO data of Dubner and Arnal (1988), indicating a low column density or else the cloud is at a velocity outside the range of 2–24 km s^{-1}. Another factor is that the south clump may have a lower emission measure and a higher temperature than the eastern knot, because the tail appears to be less dense than the east cloud. If $T_{\rm gas} > 6 \times 10^6$ K, both of these differences would also act to make the south clump less bright in the HRI bandpass. The lack of enhanced H I or CO emission makes it unlikely that the local density near the south clump could be high enough to slow the shock to the point where it was too cool to emit strongly in the HRI bandpass.

At this point, we can attempt to describe the three-

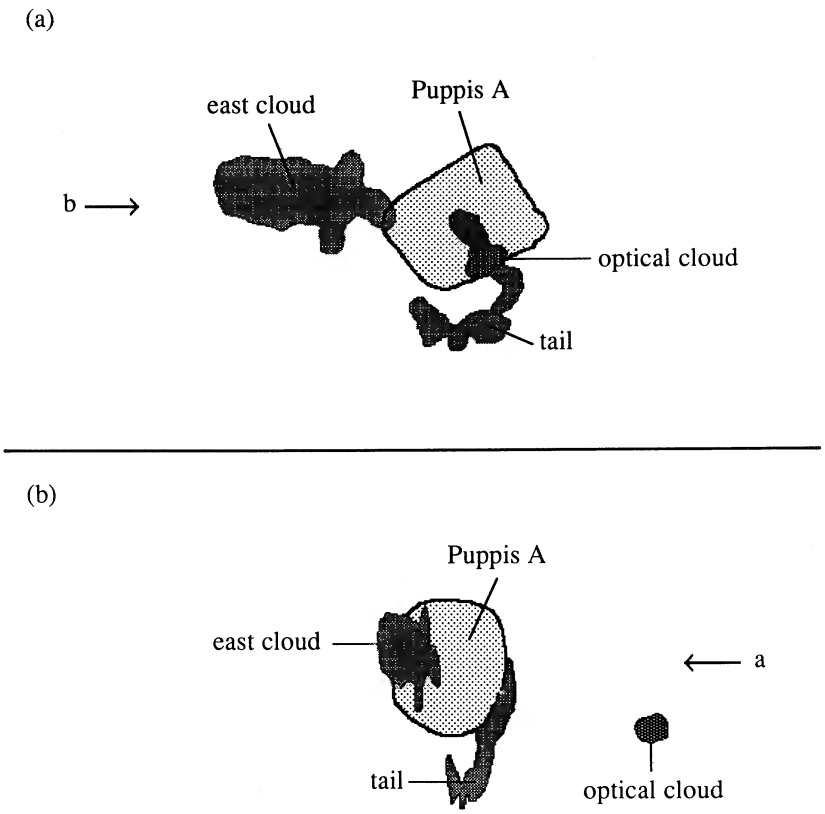

FIG. 9.—(*a*) Puppis A and surrounding clouds as seen from Earth. The dark optical cloud appears on the same line of sight as the tail and south clump. The direction from which one might see the scene sketched in (*b*), i.e., from the east, is indicated. (*b*) Puppis A and its environment as they might appear from the east. The tail has been drawn, for the sake of illustration, as if it wraps around the front side of the SNR. It is equally likely that it wraps around the back side of the SNR instead. The distance between the dark optical cloud and the SNR is unknown and not to scale. The direction from which one sees the view in (*a*), i.e., from Earth, is indicated.

dimensional structure of the interstellar medium in the vicinity of Puppis A. Figure 9 shows two views of the volume of space around Puppis A. Figure 9*a* shows the view from Earth. The shapes of the clouds and the SNR are sketched from the IR and radio data, respectively. We know that the east cloud must lie in nearly the same plane of the sky as the SNR, because its interaction with the SNR (the eastern knot) lies at the extreme edge of the remnant as opposed to being seen in projection on the face of the remnant. The east cloud may be projected slightly over the border of the SNR as suggested by the extent of the cloud in the 12 μm data, in which the cloud is still visible but the SNR is not. The ambiguity of whether this slight overlap is in front of or behind the SNR cannot be resolved. The tail extends across the face of Puppis A and, as for the overlap of the east cloud, we are unable to discern whether the tail is on the front or back side of the SNR. For clarity, we depict it in Figure 9*b* as if it wraps around the front side of the remnant. Figure 9*b* also illustrates how the interaction with the tail appears brightest at the south clump, where we view it over a longer path length. The cloud responsible for the optical absorption must lie along the line of sight to the south clump, but much closer to us than the other clouds near Puppis A.

The most enigmatic portion of Puppis A is the hook. This feature is the brightest portion of the SNR in the radio, but is only of faint or moderate brightness in the IR and X-rays. At the north end of the hook lies the east cloud, which is probably the densest portion of the ISM presently encountered by Puppis A. Just to the south of the hook lies what is probably the least dense region of the ISM near Puppis A. The low density is suggested by the lack of X-ray and IR emission from this area, the lack of radio limb brightening, and the fact that the angular radius of the radio emission (measured from the expansion center determined by Winkler *et al.* 1988) is greater in this direction than anywhere else around the SNR. Apparently the radio emission is strongly enhanced in the region of this steep density gradient between the east cloud and the region to its south, but the density of the swept-up material is still low enough that the X-ray and IR emission remain weak. If the steep gradient leads to the formation of instabilities, then the radio emission could be increased by magnetic field amplification, which would have little or no effect on the IR and X-ray emission. As the shock front of the SNR progresses into the east cloud and more mass is accumulated, the IR and X-ray emission will rise. A relatively high ratio of radio to IR emission has been found to be characteristic of the youngest SNRs (Arendt 1989). The hook may indicate that, within a single SNR, it is possible to tell more recent interactions from older events. Providing further support for this theory is the southernmost portion of the south clump. This location, which marks the most recent interaction of the SNR and the tail, also exhibits a high ratio of radio to IR emission.

V. SUMMARY

From this morphological study of Puppis A, we find that the IR data contain a great deal of information on the structure of the ISM. With the additional use of radio, optical, and X-ray

data, we are able to estimate the three-dimensional structure of the ISM in the vicinity of Puppis A. The supernova remnant is observed to be interacting with density structures in the ISM. The best example is at the location of the eastern knot, where observations clearly reveal the interface between a molecular cloud (the "east cloud") and the SNR. These interactions are evident through the large effects they have on the morphology of the remnant at all wavelengths. The infrared data alone do not establish the association between the east cloud and the SNR, but when combined with data at other wavelengths, the case is greatly strengthened. Good correlation between IR and X-ray emission across Puppis A suggests that the IR radiation is predominantly thermal emission from interstellar dust, which has been swept-up by the SNR and heated collisionally by the shocked gas.

We thank J. Meaburn for the use of his optical photograph of Puppis A. The Molonglo Observatory is funded by the Australian Research Grants Scheme, the University of Sydney Research Committee, and the Science Foundation for Physics within the University. R. G. A. has used much of the work presented here as part of a Ph.D. dissertation at the University of Illinois, and he has been supported under the NASA Graduate Student Researchers Program (Grant NGT-50152), and NASA contract JPL 958014.

REFERENCES

Arendt, R. G. 1989, *Ap. J. Suppl.*, **70**, 181.
Beichman, C. A. 1987, *Ann. Rev. Astr. Ap.*, **25**, 521.
Caswell, J. L., and Lerche, I. 1979, *M.N.R.A.S.*, **187**, 201.
Dickel, J. R., and Willis, A. G. 1980, *Astr. Ap.*, **85**, 55.
Dubner, G. M., and Arnal, E. M. 1988, *Astr. Ap. Suppl.*, **75**, 363.
Dwek, E., Petre, R., Szymkowiak, A., and Rice, W. 1987, *Ap. J. (Letters)*, **320**, L27.
Elliott, K. H., Goudis, C., and Meaburn, J. 1976, *M.N.R.A.S.*, **175**, 605.
Giacconi, R., *et al.* 1979, *Ap. J.*, **230**, 540.
Goudis, C., and Meaburn, J. 1978, *Astr. Ap.*, **62**, 283.
Green, D. A. 1988, *Ap. Space Sci.*, **148**, 3.
IRAS Catalogs and Atlases: Explanatory Supplement. 1985, ed. C. A. Beichman, G. Neugebauer, H. J. Habing, P. E. Clegg, and T. J. Chester (Washington, DC: U.S. Government Printing Office).
IRAS Point Source Catalog. 1985, Joint IRAS Science Working Group (Washington, DC: U.S. Government Printing Office).
IRAS Small Scale Structures Catalog. 1986, prepared by G. Helou and D. Walker (Washington, DC: U.S. Government Printing Office).
Kesteven, M. J., and Caswell, J. L. 1987, *Astr. Ap.*, **183**, 118.
McKee, C. F., and Ostriker, J. P. 1977, *Ap. J.*, **218**, 148.
Mills, B. Y. 1981, *Proc. Astr. Soc. Australia*, **4**, 156.
Milne, D. K. 1979, *Australian J. Phys.*, **32**, 83.
Milne, D. K., Goss, W. M., and Danziger, I. J. 1983, *M.N.R.A.S.*, **204**, 237.
Mufson, S. L., McCollough, M. L., Dickel, J. R., Petre, R., White, R., and Chevalier, R. 1986, *A.J.*, **92**, 1349.
Neugebauer, G., *et al.* 1984, *Ap. J. (Letters)*, **278**, L1.
Petre, R., Canizares, C. R., Kriss, G. A., and Winkler, P. F. 1982, *Ap. J.*, **258**, 22.
Petre, R., and Teske, R. G. 1987, *Ap. J.*, **318**, 370.
Roger, R. S., Milne, D. K., Wellington, K. J., Haynes, R. F., and Kesteven, M. J. 1984, *Proc. Astr. Soc. Australia*, **5**, 560.
Seward, F. D. 1988, in *Supernova Remnants and the Interstellar Medium*, ed. R. S. Roger and T. L. Landecker (Cambridge: Cambridge University Press), p. 115.
Straka, W. C., Dickel, J. R., Blair, W. P., and Fesen, R. A. 1986, *Ap. J.*, **306**, 266.
Szymkowiak, A. E. 1985, Ph.D. thesis, University of Maryland.
Winkler, P. F., and Kirshner, R. P. 1985, *Ap. J.*, **299**, 981.
Winkler, P. F., Tuttle, J. H., Kirshner, R. P., and Irwin, M. J. 1988, in *Supernova Remnants and the Interstellar Medium*, ed. R. S. Roger and T. L. Landecker (Cambridge: Cambridge University Press), p. 65.
Zarnecki, J. C., Culhane, J. L., Toor, A., Seward, F. D., and Charles, P. A. 1978, *Ap. J. (Letters)*, **219**, L17.

RICHARD G. ARENDT and ELI DWEK: Laboratory for Astronomy and Solar Physics, Code 685, NASA Goddard Space Flight Center, Greenbelt, MD 20771

JOHN R. DICKEL: 349 Astronomy Building, 1011 West Springfield Avenue, Urbana, IL 61801

MICHAEL J. KESTEVEN and DOUGLAS K. MILNE: Division of Radiophysics, CSIRO, P.O. Box 76, Epping, NSW 2121, Australia

ROBERT PETRE: Laboratory for High Energy Astrophysics, Code 666, NASA Goddard Space Flight Center, Greenbelt, MD 20771

ROBERT S. ROGER: Herzberg Institute of Astrophysics, Dominion Radio Astrophysical Observatory, Box 248, Penticton, BC, Canada V2A 6K3